

UC Irvine

UC Irvine Previously Published Works

Title

Cranial grafting of stem cell-derived microvesicles improves cognition and reduces neuropathology in the irradiated brain

Permalink

<https://escholarship.org/uc/item/1187f13x>

Journal

Proceedings of the National Academy of Sciences of the United States of America, 113(17)

ISSN

0027-8424

Authors

Baulch, Janet E
Acharya, Munjal M
Allen, Barrett D
et al.

Publication Date

2016-04-26

DOI

10.1073/pnas.1521668113

Peer reviewed

Cranial grafting of stem cell-derived microvesicles improves cognition and reduces neuropathology in the irradiated brain

Janet E. Baulch^{a,1}, Munjal M. Acharya^{a,1}, Barrett D. Allen^a, Ning Ru^a, Nicole N. Chmielewski^a, Vahan Martirosian^a, Erich Giedzinski^a, Amber Syage^a, Audrey L. Park^a, Sarah N. Benke^a, Vipin K. Parihar^a, and Charles L. Limoli^{a,2}

^aDepartment of Radiation Oncology, University of California, Irvine, CA 92697-2695

Edited by James E. Cleaver, University of California, San Francisco, CA, and approved February 26, 2016 (received for review November 2, 2015)

Cancer survivors face a variety of challenges as they cope with disease recurrence and a myriad of normal tissue complications brought on by radio- and chemotherapeutic treatment regimens. For patients subjected to cranial irradiation for the control of CNS malignancy, progressive and debilitating cognitive dysfunction remains a pressing unmet medical need. Although this problem has been recognized for decades, few if any satisfactory long-term solutions exist to resolve this serious unintended side effect of radiotherapy. Past work from our laboratory has demonstrated the neurocognitive benefits of human neural stem cell (hNSC) grafting in the irradiated brain, where intrahippocampal transplantation of hNSC ameliorated radiation-induced cognitive deficits. Using a similar strategy, we now provide, to our knowledge, the first evidence that cranial grafting of microvesicles secreted from hNSC affords similar neuroprotective phenotypes after head-only irradiation. Cortical- and hippocampal-based deficits found 1 mo after irradiation were completely resolved in animals cranially grafted with microvesicles. Microvesicle treatment was found to attenuate neuroinflammation and preserve host neuronal morphology in distinct regions of the brain. These data suggest that the neuroprotective properties of microvesicles act through a trophic support mechanism that reduces inflammation and preserves the structural integrity of the irradiated microenvironment.

radiation-induced cognitive dysfunction | microvesicles | dendritic complexity | human neural stem cells | neuroinflammation

With improved diagnosis and treatment, cancer survivorship continues to rise but often at the cost of quality of life. The unintended neurocognitive sequelae resulting from cranial irradiation used to treat primary and secondary malignancies of the brain are both progressive and debilitating (1, 2). Despite the recognition and prevalence of these adverse side effects, relatively few, if any, long-term satisfactory solutions exist for this unmet medical need. Past work from our laboratory has optimized transplantation parameters and established many of the long-term benefits of human stem cell-based therapies for the treatment of radiation-induced cognitive dysfunction (3–5). Cranially grafted stem cells have been shown to impart persistent improvements in behavioral performance in irradiated rats over extended postirradiation intervals (1–8 mo) using short- and long-term cognitive testing paradigms (4, 6, 7). These studies have shown that our stem cell-based approaches improve the functional plasticity of the host brain through a variety of mechanisms including (i) the suppression of neuroinflammation (5), (ii) the addition of new cells to active hippocampal circuits (4), and (iii) a long-term trophic support mechanism that facilitates the expression of activity-regulated cytoskeleton-associated protein that functions in multiple ways as a molecular determinant of memory (7). Moreover, using a distinctly different injury paradigm, stem cell grafting preserved host neuronal morphology in rats that otherwise experienced significant disruptions to dendritic complexity following a chronic chemotherapy regimen (8).

Although human stem cell therapies have proved promising for a number of clinical scenarios including the treatment of disease or traumatic injury, they are not without risk. Among the concerns regarding stem cell use is the possibility of teratoma formation and immune rejection requiring immunosuppression. One strategy to circumvent the caveats of engrafting stem cells into the irradiated brain is to transplant stem cell-derived microvesicles (MV) instead of the stem cells themselves. These small membrane-bound vesicles are generated by many cell types and contain bioactive cargo such as proteins, lipids, mRNAs, and micro-RNAs (9). MV are now recognized as regulators of biological processes, with specific cargo capable of controlling signaling and function of target cells (10). For this reason, MV represent a unique paracrine signaling mechanism with therapeutic potential. The literature demonstrates that MV are capable of effectively promoting recovery of the CNS after traumatic brain injury or stroke (11, 12). We hypothesize that this same cell-free therapeutic approach will, at least in part, mitigate radiation-induced damage to the brain by delivering beneficial cargo. As proof of principle, in this study we have grafted human neural stem cell (hNSC)-derived MV into the hippocampus of the host brain and assessed their ability to reduce neuroinflammation and protect neuronal structure, ultimately sparing the brain from the cognitive deficits induced by irradiation.

Significance

Cranial irradiation used during the clinical management of brain cancer is associated with severe cognitive decline and represents a particular concern for pediatric cancer survivors. Irradiation triggers neuroinflammation and compromises the structure of neurons, factors that are contributory if not causal to radiation-induced cognitive dysfunction. Our previous data have shown that intrahippocampal transplantation of human neural stem cells (hNSCs) could ameliorate radiation-induced behavioral deficits and improve neuronal plasticity. These beneficial neurocognitive effects were hypothesized to act through a trophic support mechanism involving the secretion of microvesicles acting on host neuronal circuitry. Here we show that cranial grafting of hNSC-derived microvesicles reverses or prevents radiation-induced cognitive dysfunction through mechanisms involving the suppression of inflammation and the preservation of host neuronal architecture.

Author contributions: J.E.B., M.M.A., V.K.P., and C.L.L. designed research; J.E.B., M.M.A., B.D.A., N.R., N.N.C., V.M., E.G., A.S., A.L.P., S.N.B., and V.K.P. performed research; J.E.B., M.M.A., B.D.A., V.K.P., and C.L.L. analyzed data; and J.E.B., M.M.A., and C.L.L. wrote the paper.

The authors declare no conflict of interest.

This article is a PNAS Direct Submission.

Freely available online through the PNAS open access option.

¹J.E.B. and M.M.A. contributed equally to this work.

²To whom correspondence should be addressed. Email: climoli@uci.edu.

This article contains supporting information online at www.pnas.org/lookup/suppl/doi:10.1073/pnas.1521668113/-DCSupplemental.

Results

Novel Place Recognition. One month after transplantation of MV, animals were habituated and tested on the novel place recognition (NPR) task (Fig. 1A). The total exploration of objects during the familiarization and test phases were found to be indistinguishable between all cohorts for this task. Group means and 95% confidence intervals (CIs) for the discrimination indices (DIs) were as follows: 0 Gy Control (Con, mean = 48.13, 95% CI = 32.48–63.78), 10 Gy irradiated (IRR, mean = 12.63, 95% CI = 8.348–33.61), and irradiated receiving MV transplantation (IRR+MV, mean = 39.32, 95% CI = 25.97–52.68). A significant overall group effect was found, $F(2, 25) = 5.651$, $P = 0.009$, for the DI to differ between groups. Following a 1-h retention interval between familiarization and test phases, IRR animals spent significantly less time exploring the novel place compared with Con ($P = 0.01$) and IRR+MV ($P = 0.05$) groups. In contrast, IRR+MV animals did not differ from Con animals. These data indicate that transplantation of MV improved spatial exploration behavior on the NPR task after irradiation compared with irradiated but nontransplanted animals.

Novel Object Recognition. After NPR testing, animals were habituated and subject to a novel object recognition (NOR) task (Fig. 1B). As before, animals explored familiar and novel objects equally during this task. The group means and 95% CIs for the DI were as follows: Con (mean = 46.43, 95% CI = 36.24–56.61), IRR (mean = 1.25, 95% CI = –18.86–21.37), and IRR+MV (mean = 38.62, 95% CI = 18.77–58.47). Again, a significant overall group effect was found, $F(2, 31) = 6.175$, $P = 0.005$, for the DIs to differ between groups. Following a 5-min retention interval between familiarization

and test phases, IRR animals spent significantly less time exploring the novel object compared with Con ($P = 0.001$) and IRR+MV ($P = 0.01$) groups. As in the prior task, the DIs for Con and IRR+MV groups were statistically indistinguishable. Thus, MV grafting improved novel object exploration behavior in irradiated animals.

Object in Place. The third open arena test used to evaluate cognitive function was the object in place (OiP) task (Fig. 1C). Total exploration times for the objects followed similar trends as those observed for the previous tests. Rats having intact cortical function exhibit a preference for objects that had been moved to a novel location. The group means and CIs for the DI in each cohort were as follows: Con (mean = 24.08, 95% CI = 16.87–31.28), IRR (mean = –14.90, 95% CI = –27.91 to –1.89), and IRR+MV (mean = 38.26, 95% CI = 32.35–44.17). The overall group effect for DI between the three cohorts was again found to differ significantly, $F(2, 31) = 52.66$, $P < 0.0001$. Following familiarization, test phases showed that IRR animals spent significantly less time exploring the novel placement of objects compared with the Con ($P = 0.001$) and IRR+MV ($P = 0.001$) groups. Once again, the Con and IRR+MV groups did not differ statistically and showed a distinct preference for those objects placed at novel locations. These data again demonstrate that cranial grafting of MV improves exploration behavior after irradiation.

Temporal Order. After OiP testing, rats were habituated and tested on the temporal order (TO) task (Fig. 1D). After familiarization with two sets of objects presented 4 h apart (sample phases 1 and 2) and 1 h after sample phase 2, rats were subjected to the test phase using one of the same objects presented in each of the earlier phases. Animals with intact perirhinal cortical function exhibit a preference for the object explored during sample phase 1 over the more recently explored, sample phase 2 object. Total exploration of the objects during the familiarization and test phases were reduced, albeit not significantly, after irradiation compared with Con and IRR+MV groups. Control and grafted cohorts were again not found to differ statistically. Although group differences did not reach significance for this task, overall trends indicate that transplantation of MV afforded some improvement in exploration behavior after irradiation.

In summary, for each open arena task, exploration ratios were normalized by the time spent at a familiar location or object by calculating the DI. In nearly every instance, a preference for novelty was found to be significantly higher for Con and IRR+MV groups in comparison with the IRR group, demonstrating the beneficial neurocognitive effects of MV transplantation (Fig. 1).

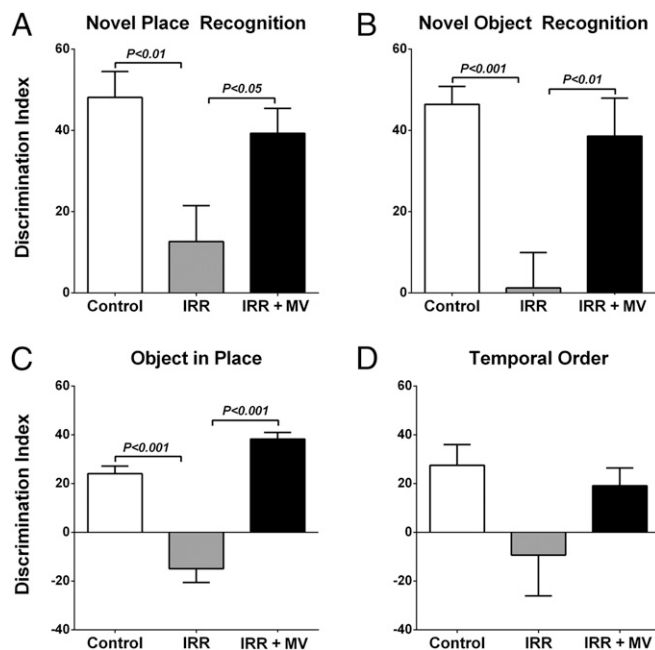


Fig. 1. hNSC cell-derived MV protect against radiation-induced cognitive dysfunction. Six-month-old ATN rats received cranial irradiation (0 or 10 Gy) and received intrahippocampal transplantation of hNSC-derived MV 2 d later. One month postimplantation, animals were administered spontaneous exploration tasks in the following order: NPR, NOR, OiP, and TO. Tendency to explore novelty (novel place or object) was calculated using the DI [(novel location exploration time/total exploration time) – (familiar location exploration time/total exploration time)] × 100. (A–C) Cranial irradiation significantly impaired exploration on NPR, NOR, and OiP tasks compared with Con and IRR+MV cohorts that were not statistically different. (D) Irradiation impaired preference of prior objects on a TO task compared with controls and grafted cohorts but was not statistically different. All data are presented as mean ± SEM ($n = 8$ –12 rats per group). P values are derived from ANOVA and Bonferroni's multiple comparisons test.

Contextual Fear Conditioning. The training, cue, and context phases of the fear conditioning (FC) task were administered over a period of 3 d. Group means and 95% CIs for posttraining and context phase freezing (percent) were as follows: Posttraining Con (mean = 97.70, 95% CI = 95.0–100.4), IRR (mean = 94.56, 95% CI = 88.67–97.24), IRR+MV (mean = 92.96, 95% CI = 88.67–97.24), Context Con (mean = 48.63, 95% CI = 32.92–64.34), IRR (mean = 25.26, 95% CI = 10.86–39.66), and IRR+MV (mean = 52.15, 95% CI = 44.01–60.30). Using repeated measures (RM) ANOVA, a significant overall Group × Phase interaction effect was found for the percent time spent freezing during the FC task (Fig. 2), $F(8, 104) = 2.196$, $P = 0.03$. RM two-way ANOVA for the context phase revealed significant differences between the IRR and Con groups ($P = 0.003$) and between the IRR and IRR+MV groups ($P = 0.001$). Groups did not differ significantly in the freezing behavior across baseline, posttraining, precue, and postcue phases, indicating a selective deficit on the hippocampal-dependent contextual memory phase of the task. During the context test phase, post hoc tests confirmed that IRR animals spent significantly less time freezing compared with the Con ($P = 0.02$) and IRR+MV ($P = 0.002$) groups, whereas the Con and IRR+MV groups did not differ. Further, because all groups showed significant increases in freezing behavior after the tone–shock pairing (posttraining phase), irradiation did not impair motor or sensory function. The fact that cued memory was intact

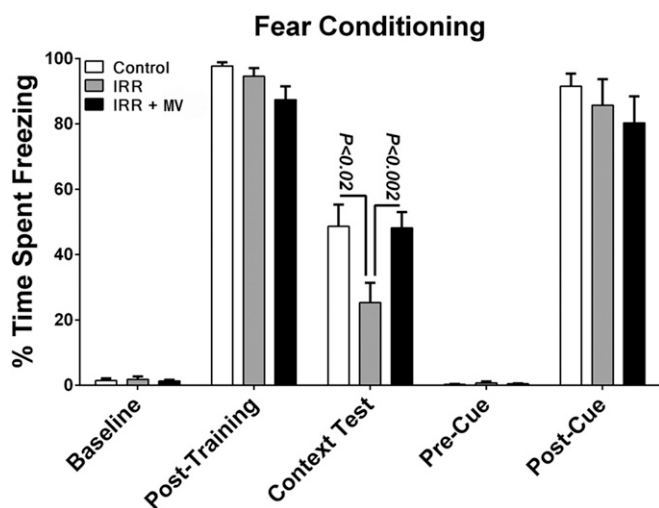


Fig. 2. MV grafting improves behavior on the hippocampal-dependent contextual FC task. The baseline freezing levels were equivalent across groups, and all groups showed increased freezing behavior following a series of five tone–shock pairings (posttraining phase). The context test was administered 24 h later, and irradiated animals showed significantly decreased freezing compared with Con. Irradiated animals receiving MV showed increased freezing behavior that was indistinguishable from the Con group (context test bars). After the initial training phase (48 h), the context was changed, resulting in a substantial reduction in freezing behavior in all groups upon sounding of the tone (cue test phase), indicating intact amygdala function. Data are presented as mean \pm SEM ($n = 8$ –12 rats per group). P values are derived from ANOVA and Bonferroni's multiple comparisons test.

also demonstrates that the acquisition of the tone–shock pairing was not impaired and that the deficit was specific to the memory of the context in which the pairing had been learned.

Graft Location of MV. The presence of grafted MV was confirmed at 2 d and 2 wk after surgery using rhodamine anti-green fluorescence protein (GFP) antibody immunofluorescence to amplify the GFP-CD63 signal (appearing as red puncta) and confocal Z-stack analysis of transplanted brains (Fig. 3). At 2 d posttransplantation, MV aggregates were found predominantly dorsal to the CA1 region of the hippocampus, in the vicinity of the needle track (Fig. 3A). Although smaller numbers of MV remained in the CA1 region of the hippocampus 2 wk postsurgery, many were found to disperse and to have migrated to the dentate gyrus (DG) region (Fig. 3B and C). Immunostaining indicated that a certain fraction of the MV cargo was internalized into host brain cells. Dual immunofluorescence staining for MV cargo along with neuron-specific nuclear antigen (NeuN) or glial fibrillary acidic protein (GFAP) provided evidence, albeit circumstantial, indicating fusion and internalization of MV cargo by both neuronal and astrocytic cell types (Fig. 3D and E, respectively).

Neuroinflammation. Previously, we demonstrated that exposure to cranial irradiation or systemic chemotherapy increased neuroinflammation (5, 8). To assess the impact of hNSC-derived MV on inflammation in the brain, activated microglia (ED-1⁺ cells) were quantified using unbiased stereology throughout the distinct brain regions including the hippocampus, neocortex (layer II/III), and amygdala (Fig. 4). A significant overall group effect was found for the number of activated microglia in the hippocampal dentate hilus (DH), $F(2, 6) = 14.32$, $P = 0.005$, granular cell layer (GCL), $F(2, 6) = 14.17$, $P = 0.005$, and the CA1/3 subfields, $F(2, 6) = 30.70$, $P = 0.0007$, in addition to cortical layer II/III, $F(2, 8) = 13.59$, $P = 0.003$, and the amygdala, $F(2, 8) = 18.00$, $P = 0.001$, where radiation exposure induced 4–5-fold increases in ED-1⁺ cells, $F(2, 6) = 21.47$, $P = 0.002$ (Fig. 4D). However, MV

grafting resulted in a significant reduction in the number of activated microglia throughout the hippocampus, reducing the yield of ED-1⁺ cells to below control levels (29%, 12%, and 45% lower than control levels for the DH, DG, and CA3/1 regions, respectively). Similar reductions in activated microglia were observed in the cortex (layer II/III) and amygdala. These data demonstrate that MV grafting could significantly suppress radiation-induced activation of microglia in regions of the brain both proximal and distal to the engraftment site.

Neuronal Morphometry. Our past studies have shown that cranial irradiation could significantly disrupt components of neuronal architecture including dendritic length, volume, and complexity (13, 14). To determine the potential impact of MV grafting on neuronal structure, Golgi–Cox-impregnated sections were used in detailed morphometric analyses of GCL neurons in the DG.

Panoramic bright field images of Golgi–Cox-impregnated neurons in the DG reveal the marked impact of cranial irradiation and MV grafting. Compared with controls, neuronal complexity is severely compromised after radiation exposure, an adverse effect that is reversed by MV grafting (Fig. 5A–C). Representative Golgi–Cox-stained neurons (Fig. 5D–F) and Neurolucida tracings (Fig. 5G–I) are shown for each cohort. Quantification of dendritic parameters on GCL neurons revealed the adverse effects of radiation and the beneficial effects of MV on neuronal structure (Fig. 5J–L). Significant overall group effects were found for dendritic length, $F(2, 9) = 9.022$, $P = 0.007$, volume, $F(2, 9) = 74.59$, $P = 0.0001$, and complexity, $F(2, 9) = 42.25$, $P = 0.0001$, clearly demonstrating that cranial irradiation significantly compromised neuronal structure and that MV transplantation protected against this effect. Although MV transplantation did not restore dendritic volume to control levels, it did confer significant protection ($P = 0.01$). Transplantation was more effective in protecting other dendritic parameters, restoring dendritic length to 89% of control levels ($P = 0.01$) and restoring dendritic complexity to greater than control levels ($P = 0.001$). For each of these endpoints, data show that MV grafting preserved the structure of hippocampal GCL neurons following irradiation.

Discussion

Despite the considerable promise of using stem cells to hasten the recovery of radiation-induced normal tissue injury (for review, see ref. 15), issues concerning ethics, immunorejection, and teratoma formation remain significant concerns. To circumvent some of these potential confounders and to establish a potentially novel therapeutic strategy for ameliorating radiation-induced cognitive dysfunction, MV were substituted for hNSC in cranial grafting procedures following head-only irradiation. Here we report the advantages of MV transplantation, which was found to be as effective as hNSC in reversing many of the adverse indications of cranial irradiation.

Rats receiving head-only irradiation and MV grafting were found to exhibit improved performance, as assessed by four well-characterized and widely used cognitive tasks (Fig. 1). These spontaneous exploration tasks interrogate various combinations of hippocampal and cortical learning and memory, providing a quantifiable readout of behavioral performance between cohorts. Data from the NPR, NOR, and OiP tasks indicate that irradiation disrupts hippocampal, medial prefrontal cortex, and perirhinal cortex circuitry, which impacts spatial, episodic, and associative recognition memory function (16–19). The use of MV isolated from hNSCs was found to elicit significant improvements on the NPR, NOR, and OiP tasks, with a trend showing similar cognitive benefits on the TO task when assessed 4–6 wk following irradiation and transplantation procedures (Fig. 1). In contrast to those animals receiving irradiation only, the performance of animals receiving irradiation and MV grafting was indistinguishable from sham surgery controls, where both controls and transplanted animals showed significant preference for exploring the novel place and/or object. Task redundancy and/or testing fatigue may have contributed to the loss of interest to explore novelty during the

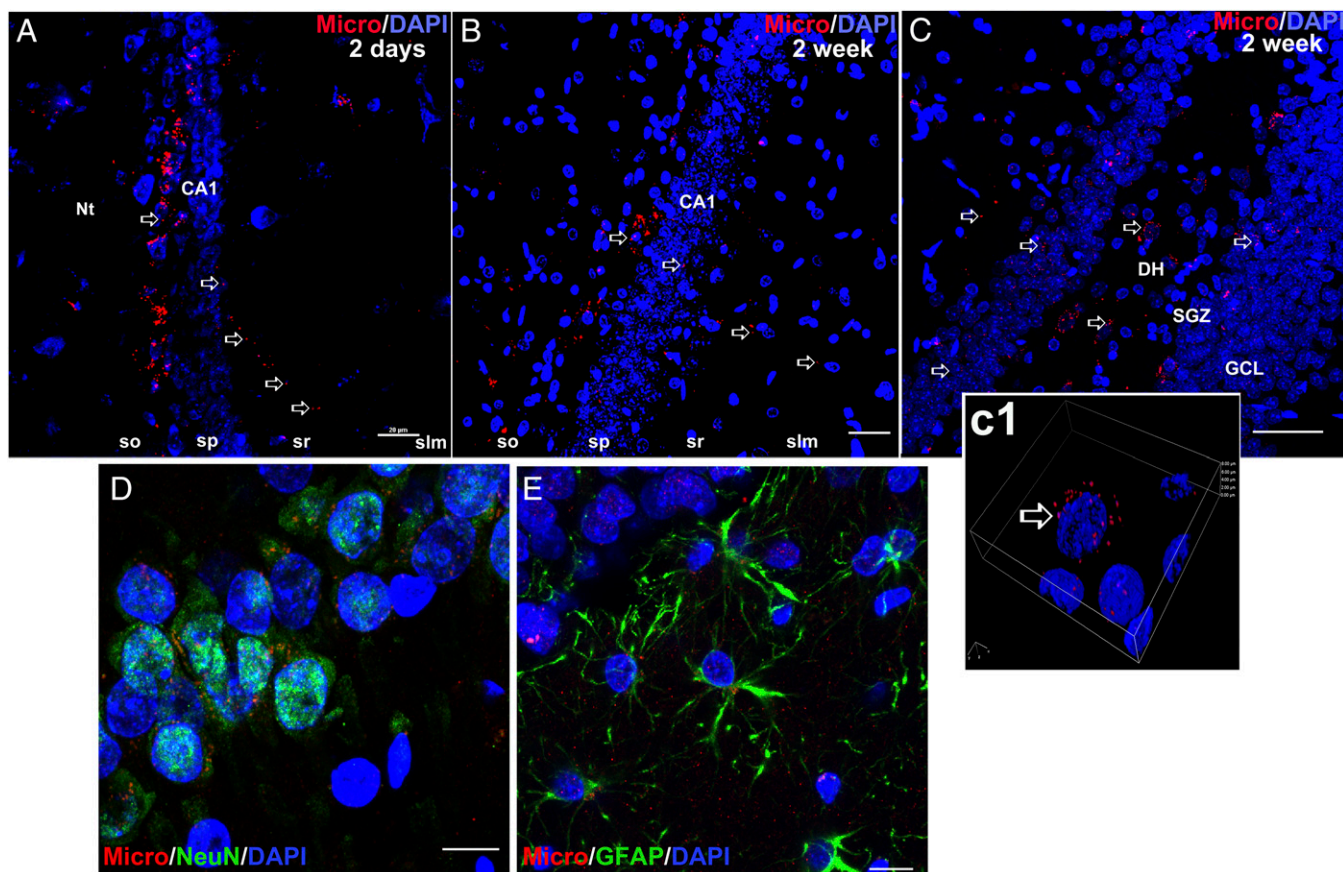


Fig. 3. MV location in the irradiated brain. (A) Two days posttransplantation, the majority of the grafted MV were found in aggregates near the needle track (Nt), dorsal to the CA1 region of the hippocampus, with some vesicles beginning to migrate ventrally. (B) At 2 wk after transplantation, MV were still located diffusely in the CA1 region as well as in the (C) hippocampal DH, subgranular zone (SGZ), and the GCL. High-power imaging (60 \times) shows that the MV are likely associated with cellular cytoplasm (inset c1). (D and E) Immunofluorescence staining indicates that MV have been taken up by both mature neurons (NeuN) and astroglia (GFAP). SLM, stratum lacunosum moleculare; SO, stratum oriens; SP, stratum pyramidale; SR, stratum radiatum. [Scale bars, 20 μ m (A–C) and 5 μ m (c1, D, and E).]

final task, thereby confounding the assignment of significant differences between groups.

Irradiated animals that were interrogated using a contextual FC task were found to spend significantly less time engaged in

freezing behavior than controls during the context phase of the task (Fig. 2). These data suggest that irradiation disrupted long-term (24-h) memory for the shock–context association, which has been shown to rely on intact hippocampal function (20).

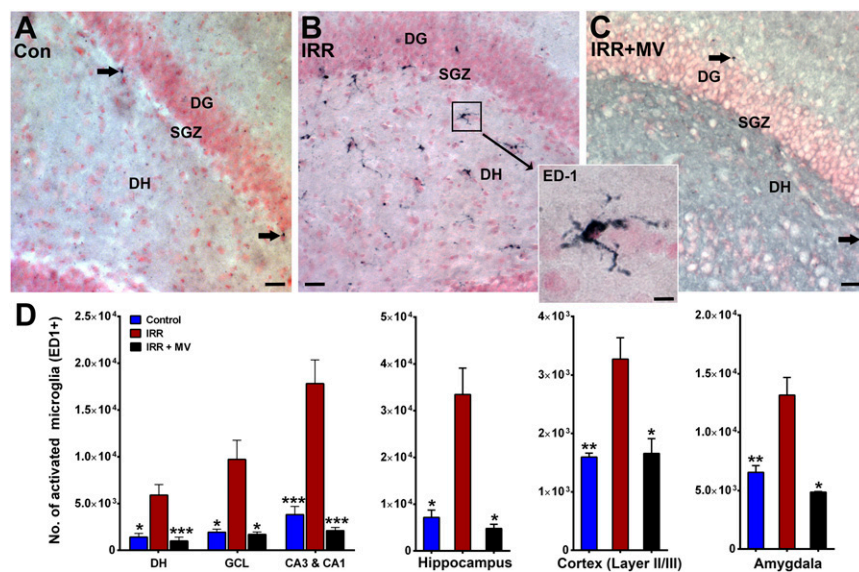


Fig. 4. MV grafting reduces the number of activated microglia. (A–C) Immunohistochemical analysis demonstrates that, compared with Con, IRR leads to increased microglial activation (ED-1⁺, black Vector SG staining and pink nuclear fast red counterstain; *inset*) that is reduced to control levels in IRR+MV animals. Representative images show the presence of activated microglia in the hippocampal subfields of the DG, SGZ, and DH. (D) Stereology quantification of activated microglia using an Optical Fractionator shows that, compared with controls, irradiation significantly increased the number of activated microglia in all regions of the brain evaluated. Compared with the IRR cohort, IRR+MV animals had significantly lower numbers of activated microglia in all hippocampal subfields, cortex (layer II/III), and amygdala. Numbers of activated microglia in each region were comparable to or lower than untreated controls. All data are presented as mean \pm SEM ($n = 3$ rats per group). * $P = 0.02$, ** $P = 0.01$, *** $P < 0.001$ compared with the control group (ANOVA and Bonferroni's multiple comparisons test). [Scale bars, 50 μ m (A–C) and 5 μ m (*inset*).]

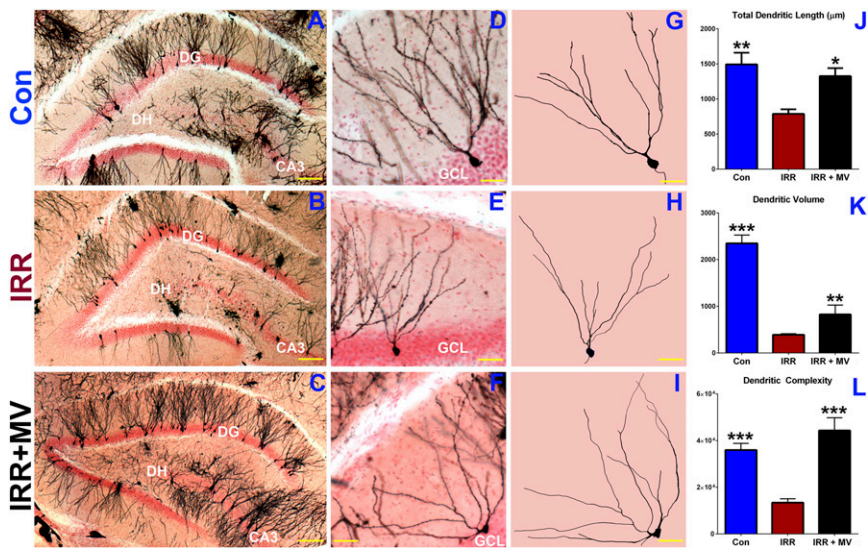


Fig. 5. MV grafting preserves granule cell neuronal morphology in the DG. (A–C) Representative images of Golgi–Cox-impregnated hippocampal tissue sections from Con, IRR, and IRR+MV illustrate the gross disruption of neuronal structure (black) in the hippocampal DG (nuclear fast red counterstained) after cranial irradiation that is resolved in animals receiving MV. (D–F) Representative GCL neurons and corresponding NeuroLucida tracing (G–I) from each cohort are shown. (J–L) Structural parameters of dendritic morphology (length, volume, complexity) quantified in each cohort demonstrate that radiation-induced reductions in dendritic morphology were ameliorated by MV grafting. Data are presented as mean \pm SEM ($n = 4$ rats per group). * $P = 0.05$, ** $P = 0.01$, *** $P = 0.001$ (ANOVA and Bonferroni's multiple comparisons test). [Scale bars, 50 μm (A–C) and 20 μm (D–I).]

Interestingly, animals engrafted with MV following irradiation demonstrated intact freezing behavior and were statistically indistinguishable from controls in their contextual fear memory. The initial acquisition of the conditioned freezing response was not impacted in any of the cohorts (similar posttraining), nor was amygdala function (similar cue test) (20). These data indicate that radiation-induced deficits in hippocampal function could be ameliorated using MV and were functionally equivalent to hNSCs used under similar conditions in many of our past studies (4, 8).

Our findings clearly demonstrate that cranially grafted MV can afford functional improvements in cognition following head-only irradiation. To dissect the potential mechanisms underlying these beneficial neurocognitive effects, we followed the time course and in vivo distribution of engrafted MV containing a fluorescently labeled marker (CD63-GFP⁺). The marker was clearly visible along the needle track and in close proximity to the injection site 2 d following transplantation (Fig. 3A) and was found to penetrate throughout various hippocampal subfields by 2 wk (Fig. 3B and C). Further analysis also revealed significant nuclear colocalization in mature neurons (Fig. 3D) and astrocytes (Fig. 3E), suggesting that MV fused with and released their cargo into cells within the host brain. These data indicate that MV are taken up by neuronal and astrocytic cell types, but do not preclude an influence of MV-mediated signaling on other cell types in the brain. Although not without caveats and despite uncertainty about target cell specificity, MV cargo can persist within the host brain and exert neuromodulatory effects capable of impacting neurotransmission.

Past work from others and us has shown that irradiation leads to persistent and temporally complex patterns of neuroinflammation (7, 21, 22). We have shown that transplantation of hNSCs can reduce radiation-induced inflammation to below background levels when assessed 1 or 8 mo after irradiation (5, 7). Current findings indicate that similar results can be obtained with MV grafting, where increased numbers of activated microglia found after irradiation were significantly reduced in the neocortex (layer II/III), hippocampus, and amygdala, which is located distal to the needle track (Fig. 4). The correlation between reduced yields of activated microglia and improved cognition in grafted cohorts corroborates much of our past data (5, 7, 8) and suggests at least one mechanism by which cranially grafted MV impart their beneficial neurocognitive effects.

There has been a growing realization that activated microglia play an integral role in synaptic remodeling, in part mediated by their capability to prune dendritic arbors and spines (23, 24). Persistent inflammation caused by age and disease elicits chronic activation of microglia that can reshape the synaptic landscape

and compromise cognition (24). Mice depleted of microglia retain higher levels of dendritic spine density and suffer few if any adverse neurocognitive outcomes (25). To ascertain the potential functional consequences of MV-mediated reductions in activated microglia, experimental cohorts were subjected to Golgi staining for the structural assessment of GCL neurons in the DG of the hippocampus. Compared with controls, quantification of neuronal architectural parameters revealed significant reductions in dendritic arborization following irradiation (Fig. 5). Overall, dendritic length, volume, and complexity were reduced significantly 6 wk after exposure, effects that were ameliorated in cohorts receiving MV transplantation. Animals treated with MV showed marked increases in dendritic arborization, reflecting either increased sprouting stimulated by grafting or reduced dendritic pruning, possibly due to the suppression of activated microglia. In either case, data clearly demonstrate that MV grafting either protected host neuronal structure or promoted its recovery following irradiation.

Stem cell-based therapies have received significant attention due to their realized or potential promise in alleviating virtually any disease, degenerative, or age-related disorder (8, 26, 27). Much of this work has also highlighted the importance of trophic support, particularly for the longer-term recovery from normal tissue injury (6, 7, 15). Although the mechanisms underlying the beneficial effects of stem cell transplantation are certain to be complex and multifaceted, present findings suggest that secreted MV likely play an important role in mediating trophic support derived from multipotent stem cells. MV contain a wealth of bioactive cargo ranging from long noncoding to micro-RNAs, neurotrophic factors, membrane-bound receptors, and other small molecules capable of playing a variety of neuromodulatory roles (23, 24). These factors could directly or indirectly stimulate astroglial-derived plasticity or neuronal support through enhanced remyelination, neurogenesis, immunomodulation, the delivery of antioxidants, the secretion of neurotrophic factors, addition of membrane-bound receptors, the replenishment of neurotransmitter pools, or improved synaptic connectivity by attenuating intercellular signaling and the degradation of neuronal structure after irradiation (24). Furthermore, the neurocognitive benefits of MV transplantation are likely to be enhanced when provided before the onset of more irreversible neuropathology. Although the specific factor or combination of MV-derived molecules mediating neuroprotective phenotypes was not identified, MV do provide attractive transplantation alternatives to stem cells. Engraftment of MV to restore cognition avoids the risk of teratoma formation in the brain and minimizes host graft rejection, obviating the need for administering complex immunosuppression protocols. Although longer-term studies are needed to elucidate the potential therapeutic efficacy of

MV grafting, current proof-of-principle studies demonstrate the promise of using MV to reduce the normal tissue complications associated with the radiotherapeutic management of cancer.

Methods

Detailed methods and procedures regarding cognitive testing, stem cell and MV isolation, and morphometric and stereological assessments of neurons and microglia are provided in [Cognitive Testing](#).

Animals and Irradiation. All animal procedures are in accordance with NIH and were approved by the University of California Institutional Animal Care and Use Committee. Four-month-old male immunodeficient athymic nude (ATN) rats (Cr:NIH-Foxn1^{nu}, strain 316; Charles River) were maintained in sterile housing conditions (20 °C ± 1 °C; 70% ± 10% humidity; 12 h:12 h light and dark cycle) and had free access to sterilized diet and water. The ATN rats were divided into three experimental groups ($n = 8$ –12 per group): 0 Gy receiving sham surgery (Con), 10 Gy head-only irradiation receiving sham surgery (IRR), and 10 Gy head-only irradiation receiving MV grafting (IRR+MV). For cranial irradiation, animals were anesthetized [2.5% (vol/vol) isoflurane/oxygen], placed ventrally on the treatment table (XRAD 320 irradiator; Precision X-Ray) without restraint, and positioned under a collimated (1.0 cm² diameter) beam for head-only irradiation delivered at a dose rate of 1.0 Gy/min.

hNSC Culture, MV Isolation, and Characterization. The use of hNSCs was approved by the Institutional Human Stem Cell Research Oversight Committee. The validation, expansion, and characterization of hNSCs (ENStem-A; EMD Millipore) followed previously published procedures (4, 28). MV were isolated and purified from conditioned hNSC culture medium by ultracentrifugation (29) and characterized using a NanoSight 3000 (Malvern Instruments). The location of engrafted MV was determined using fluorescently labeled MV (CD63-GFP⁺).

Transplantation Surgery. At 2 d postirradiation, each rat received bilateral, intrahippocampal transplantation of MV suspended in vehicle (hibernation buffer) using a 33-gauge microsyringe at an injection rate of 0.25 mL/min. Each hippocampus received four distinct injections of MV (~1.0 × 10¹⁰ in 2 μL) per hemisphere using precise stereotaxic coordinates, as described previously (3). Sham surgery controls received equal volumes of sterile vehicle at the same stereotaxic coordinates. Animals were anesthetized using isoflurane/oxygen [5% (vol/vol) induction, 2.5% (vol/vol) maintenance; VetEquip].

Cognitive Testing. To evaluate the outcome of MV transplantation on cognitive function, rats from each group were subjected to cognitive testing 1 mo

after transplantation surgery. Cognitive testing was conducted over 3 wk and included four different open arena tasks followed by contextual and cued FC as described in detail previously (8, 30).

Tracking MV Engraftment. The intracranial location of GFP⁺-engrafted MV was followed 2 d and 2 wk following surgical transplantation. Animals were processed for immunohistochemistry to determine the time-dependent distribution and intracellular location of fluorescently labeled MV cargo. For further details, refer to [Cognitive Testing](#).

Neuroinflammation. Following cognitive testing, animals were killed and perfused with 4% (wt/vol) paraformaldehyde/PBS. Animals subjected to behavioral testing were segregated equally for morphometric or immunohistochemical analyses ($n = 4$ –8 per group), and brain tissues were processed for coronal sectioning using a cryostat. Immunostaining for activated microglia (ED-1⁺ cells) was carried out on serial sections (30 μm) as described previously (5). To facilitate color development, ABC Elite and Vector SG kits were used according to the manufacturer's instructions (Vector Laboratories). Sections were mounted on gelatin-coated slides, air-dried, dehydrated, and counterstained with nuclear fast red (Vector Labs). To determine the number of activated microglia (ED-1⁺), the DH, DG, and CA3 and CA1 regions of the hippocampus, neocortex (layer II/III, 1,000 × 500 μm), and amygdala were analyzed by stereology.

Neuron Structure Analysis. Extracted brains were subjected to Golgi–Cox impregnation and staining of neurons as per the manufacturer's instructions (SuperGolgi kit, Bioenno Tech.), sectioned (150 μm), and counterstained by nuclear fast red. The morphometric analysis of mature neurons in the hippocampal DG was carried out as described previously (8).

Statistics. Statistical analyses were carried out using GraphPad Prism (v6). One-way ANOVA was used to assess significance between groups. When overall group effects were found to be statistically significant, a Bonferroni multiple comparisons test was used to compare the individual groups. For analysis of FC data, RM two-way ANOVAs were performed. All analyses considered a value of $P \leq 0.05$ to be statistically significant.

ACKNOWLEDGMENTS. This work was supported by Defense Threat Reduction Agency Grant HDTRA 1-13-1-0022 (to C.L.L.), NIH National Institute of Neurological Disorders and Stroke (NINDS) Grant R01 NS074388 (to C.L.L.), American Cancer Society Grant UCI-IRG-98-279-08 (to M.M.A.), University of California, Irvine Institute for Clinical and Translational Science KL2 Award KL2TR001416 (to M.M.A.), and NASA Grant NNX13AK69G (to J.E.B.).

- Meyers CA (2000) Neurocognitive dysfunction in cancer patients. *Oncology (Williston Park)* 14(1):75–79; discussion 79, 81–82, 85.
- Butler JM, Rapp SR, Shaw EG (2006) Managing the cognitive effects of brain tumor radiation therapy. *Curr Treat Options Oncol* 7(6):517–523.
- Acharya MM, et al. (2009) Rescue of radiation-induced cognitive impairment through cranial transplantation of human embryonic stem cells. *Proc Natl Acad Sci USA* 106(45):19150–19155.
- Acharya MM, et al. (2011) Human neural stem cell transplantation ameliorates radiation-induced cognitive dysfunction. *Cancer Res* 71(14):4834–4845.
- Acharya MM, et al. (2015) Defining the optimal window for cranial transplantation of human induced pluripotent stem cell-derived cells to ameliorate radiation-induced cognitive impairment. *Stem Cells Transl Med* 4(1):74–83.
- Acharya MM, Martirosian V, Christie LA, Limoli CL (2014) Long-term cognitive effects of human stem cell transplantation in the irradiated brain. *Int J Radiat Biol* 90(9):816–820.
- Acharya MM, Rosi S, Jopson T, Limoli CL (2015) Human neural stem cell transplantation provides long-term restoration of neuronal plasticity in the irradiated hippocampus. *Cell Transplant* 24(4):691–702.
- Acharya MM, et al. (2015) Stem cell transplantation reverses chemotherapy-induced cognitive dysfunction. *Cancer Res* 75(4):676–686.
- Colombo M, Raposo G, Théry C (2014) Biogenesis, secretion, and intercellular interactions of exosomes and other extracellular vesicles. *Annu Rev Cell Dev Biol* 30:255–289.
- EL Andaloussi S, Mäger I, Breakefield XO, Wood MJ (2013) Extracellular vesicles: Biology and emerging therapeutic opportunities. *Nat Rev Drug Discov* 12(5):347–357.
- Zhang Y, et al. (2015) Effect of exosomes derived from multipotent mesenchymal stromal cells on functional recovery and neurovascular plasticity in rats after traumatic brain injury. *J Neurosurg* 122(4):856–867.
- Xin H, et al. (2013) Systemic administration of exosomes released from mesenchymal stromal cells promote functional recovery and neurovascular plasticity after stroke in rats. *J Cereb Blood Flow Metab* 33(11):1711–1715.
- Parihar VK, Limoli CL (2013) Cranial irradiation compromises neuronal architecture in the hippocampus. *Proc Natl Acad Sci USA* 110(31):12822–12827.
- Parihar VK, et al. (2015) Persistent changes in neuronal structure and synaptic plasticity caused by proton irradiation. *Brain Struct Funct* 220(2):1161–1171.
- Benderitter M, et al. (2014) Stem cell therapies for the treatment of radiation-induced normal tissue side effects. *Antioxid Redox Signal* 21(2):338–355.
- Mumby DG, Gaskin S, Glenn MJ, Schramek TE, Lehmann H (2002) Hippocampal damage and exploratory preferences in rats: Memory for objects, places, and contexts. *Learn Mem* 9(2):49–57.
- Save E, Buhot MC, Foreman N, Thinus-Blanc C (1992) Exploratory activity and response to a spatial change in rats with hippocampal or posterior parietal cortical lesions. *Behav Brain Res* 47(2):113–127.
- Barker GR, Bird F, Alexander V, Warburton EC (2007) Recognition memory for objects, place, and temporal order: A disconnection analysis of the role of the medial prefrontal cortex and perirhinal cortex. *J Neurosci* 27(11):2948–2957.
- Barker GR, Warburton EC (2011) When is the hippocampus involved in recognition memory? *J Neurosci* 31(29):10721–10731.
- Phillips RG, LeDoux JE (1992) Differential contribution of amygdala and hippocampus to cued and contextual fear conditioning. *Behav Neurosci* 106(2):274–285.
- Greene-Schloesser D, et al. (2012) Radiation-induced brain injury: A review. *Front Oncol* 2:73.
- Chiang CS, et al. (1997) Delayed molecular responses to brain irradiation. *Int J Radiat Biol* 72(1):45–53.
- Rajendran L, et al. (2014) Emerging roles of extracellular vesicles in the nervous system. *J Neurosci* 34(46):15482–15489.
- Kalani A, Tyagi A, Tyagi N (2014) Exosomes: mediators of neurodegeneration, neuroprotection and therapeutics. *Mol Neurobiol* 49(1):590–600.
- Rice RA, et al. (2015) Elimination of microglia improves functional outcomes following extensive neuronal loss in the hippocampus. *J Neurosci* 35(27):9977–9989.
- Blurton-Jones M, et al. (2009) Neural stem cells improve cognition via BDNF in a transgenic model of Alzheimer disease. *Proc Natl Acad Sci USA* 106(32):13594–13599.
- Boison D (2009) Engineered adenosine-releasing cells for epilepsy therapy: Human mesenchymal stem cells and human embryonic stem cells. *Neurotherapeutics* 6(2):278–283.
- Acharya MM, et al. (2010) Consequences of ionizing radiation-induced damage in human neural stem cells. *Free Radic Biol Med* 49(12):1846–1855.
- Théry C, Amigorena S, Raposo G, Clayton A (2006) Isolation and characterization of exosomes from cell culture supernatants and biological fluids. *Curr Protoc Cell Biol* Chapter 3:Unit 3.22.
- Christie LA, et al. (2012) Impaired cognitive function and hippocampal neurogenesis following cancer chemotherapy. *Clin Cancer Res* 18(7):1954–1965.

Supporting Information

Baulch et al. 10.1073/pnas.1521668113

Cognitive Testing

All trials were hand scored by an independent observer blind to the experimental groups, where the average of those scores was used to compute all behavioral data. The order of open arena testing consisted of NPR, followed by an NOR, an OiP, and then a TO task. For all arena tasks, a positive score was counted only when the nose of the rat was within 1 cm and pointed in the direction of the object. Behavioral data for the spontaneous exploration tasks are presented as a DI and calculated as [(novel location exploration time/total exploration time) – (familiar location exploration time/total exploration time)] × 100. A positive score indicates that rats spent more time exploring novelty (i.e., switched objects or locations), whereas a negative score indicates that rats exhibited little if any preference for exploring novelty. The FC task was administered in three sequential phases over 3 d, including a training phase, a context test, and a cue test as described previously (30).

The NPR task provides an assessment of spatial recognition memory that relies on intact hippocampal function. The effects of irradiation and MV engraftment on hippocampal function were evaluated 1 mo postsurgery by the NPR task. Spatial recognition memory during the spontaneous exploration of object placement relies on intact hippocampal function (16, 17). The behavior task setup for NPR including testing room, arenas, tracking software, and objects was as described previously (4, 30). Animals were habituated for 2 consecutive days in the open field arenas without any objects for 20 min for acclimatization to the testing rooms. The following day the familiarization and 1-h test phases were administered. Identical plastic blocks with metal bottoms were used as objects (8 × 3 × 10 cm high), which were placed 27 cm from opposing corners of the open field and secured using rare earth magnets placed beneath arena boxes. After 5 min of exploration in the familiarization phase, rats were returned to the holding cage for a 1-h retention interval. Following the 1-h delay, placement of one of the objects was moved to an open corner at a distance of 18 cm from the arena wall (novel place), whereas the other block remained at its former spatial location (familiar place). Rats were allowed to explore freely for 3 min. Following the 1-h test phase, rats were returned to their home cages. For all phases, the “head direction to zone” function in Ethovision XT software was used to track object exploration. A rat was considered to be exploring a block when its head was oriented toward it and its nose was within a 4-cm radius. In addition, an observer blind to the experimental conditions confirmed the automated tracking results independently. The NOR task followed a similar protocol, with the exception of a novel object instead of a novel place, as described (18, 19).

The OiP task is dependent on intact hippocampal function and also relies on the prefrontal and perirhinal cortices (18, 19). Rats were rehabilitated (10 min/day 1) and on the following day exposed to four objects of varying size, color, and shape for 5 min (familiarization). Rats were returned to their home cage (5 min), during which time two of the four objects switched locations. Rats were then returned to the arena for 5 min of exploration (testing). Similar to the OiP task, the TO task interrogates perirhinal and prefrontal cortices along with hippocampal function, and damage to any of these brain regions has the potential to elicit performance decrements (18, 19). For the TO task, animals were habituated (10 min) 1 d before testing. On the day of testing, animals were placed in the arena with two identical objects for 5 min (familiarization). Animals were reintroduced (4 h later) in the same arena and allowed to familiarize (5 min) with two new (but identical) objects placed in the exact same positions. Animals were finally

reintroduced (1 h later) for exploration testing (5 min) of the prior arrangement of objects, in which one was substituted for the original object presented 5 h before.

Characterization of hNSCs. hNSCs were obtained from the ENStem-A cell line (Millipore), originally derived from human embryonic stem cell line H9. Cells were passaged (passage number 1) on poly-L-ornithine (20 μg/mL; Sigma-Aldrich) and laminin (5 μg/mL, Sigma-Aldrich)-coated flasks in EnStem-A neural expansion media (Millipore) containing neurobasal media supplemented with L-glutamine (2 mM; Invitrogen), bFGF (20 ng/mL; Millipore), and B27 and LIF (Leukemia Inhibitory Factor; Millipore). Monolayers of hNSCs were passaged every other day (1:2) and doubled every 28 h. Cells were maintained in a multipotent state at passage numbers between 5–10 during the course of MV isolation and confirmed by immunostaining against Sox2 and nestin as detailed previously (28).

MV Isolation and Characterization. MV were isolated from the conditioned hNSC culture medium as described in detail (29). Briefly, large dead cells and cell debris were eliminated using successive centrifugations using increasing speeds (300 × g, 5 min; 2,000 × g, 10 min; 10,000 × g, 30 min; all at 4 °C). At each step the pellet was discarded and the supernatant carried forward. Vesicles were pelleted by ultracentrifugation using 100,000 × g (70 min, 4 °C). The pellet was then washed in sterile PBS to remove contaminating proteins and repelleted by centrifugation at 100,000 × g for an additional 70 min. MV quantity and size were determined using a NanoSight 3000 equipped with a 532-nm laser and diluted to deliver ~1 × 10¹⁰ MV per injection site. The mean MV size was 191 nm.

Following engraftment, animals were euthanized (isoflurane) followed by intracardiac perfusion (4% PFA), and brain tissues were processed for coronal sectioning using a cryostat (Leica Microsystems). Serial sections (30 μm) were washed with Tris-buffered saline and blocked in 2% (wt/vol) bovine serum albumin (BSA) with 0.01% Triton-X 100 in Tris-buffered saline (Tris-A). For the detection of GFP alone, tissues were incubated overnight in a GFP primary antibody (chicken anti-GFP, 1:500 in 2% BSA and Tris-A; Aves Labs Inc.). The following day, sections were washed and labeled with rabbit anti-chicken rhodamine (1:250 in 1% BSA and Tris-A; EMD Millipore). After washing, sections were mounted onto gelatin-coated slides and counterstained with DAPI. For dual staining of GFP and NeuN or GFAP, the above methods were used along with mouse anti-NeuN primary antibody (1:500; EMD Millipore) or mouse anti-GFAP primary antibody (1:500; EMD Millipore) labeled with donkey anti-mouse Alexa Fluor 488 (1:500; Life Technologies).

Fluorescent Labeling of MV. HEK293 cells were transfected using the lentivirus-based CD63-GFP plasmid (pCT-CD63-GFP, Cyto-Tracer, SBI) along with the lentivirus packaging plasmids (pLP1, pLP2, pL/VSVG, ViraPower Lentiviral Expression System; Invitrogen, Life Technologies). The supernatant with CD63-GFP lentiviral particles was harvested and GFP expression verified by fluorescence microscopy. hNSCs were transfected with the particles and cultured under puromycin selection. Optimal expression was observed 5–7 d posttransfection. Fluorescently labeled MV were purified and prepared for engraftment from hNSC culture medium as described above and transplanted as described in transplantation surgery methods.

Golgi–Cox Staining and Granule Cell Neuron Morphology. Animals subjected to behavioral testing were segregated equally for morphometric or immunohistochemical analyses. Extracted brains were subjected to Golgi–Cox impregnation and staining of neurons as per the manufacturer’s instructions (SuperGolgi kit, Bioenno Tech.), sectioned (150 μM), and counterstained by nuclear fast red (Vector Labs). For morphometric analyses, apical and basal dendrites were traced on neurons within the DG and CA1 subfields of the hippocampus. All analyses were conducted blind from coded slides. Neurons (6–8 per region per animal; 4 total animals) were analyzed that satisfied the following criteria: (i) uniform Golgi staining throughout the dendritic tree, (ii) absence of truncated/severed dendrites, and (iii) minimal structural overlap with neighboring neurons.

Neurons satisfying the foregoing criteria were traced using a 100 \times oil immersion objective lens (Nikon), a computerized stage (BioPrecision 2; Ludl), and NeuroLucida software (v11; MicroBrightfield, Inc.). Morphological parameters that were quantified included total dendritic length, branch points, volume, dendritic complexity, and Sholl analysis, performed using the Neuroexplorer component of the NeuroLucida program. Dendritic complexity was determined by the following equation: $(\Sigma \text{branch tip orders} + \text{number of branch tips}) \times (\text{total dendritic length} / \text{total number of primary dendrites})$. Sholl analysis used a series

of concentric circles (50 μm apart) to calculate the number of dendritic intersections as a function from distance to the soma.

ED-1 Stereology. Stereologic quantification was used to determine the number of activated microglia (ED-1⁺) in the hippocampus after completion of behavior testing. Every 10th section through the entire hippocampus was processed for ED-1 immunohistochemistry. Stereological assessment was conducted using a Nikon microscope (Nikon TE2000-E) equipped with a MBF color digital camera, 100 \times (oil immersion, 1.30 N.A.; Zeiss) objective lens, three-axis motorized stage (Bio Precision 2; Ludl), and an optical fractionator probe (StereoInvestigator; MBF Bioscience). Systemic random sampling and image stack analysis modules were used to acquire batch images through the anterior–posterior planes of the hippocampus. The acquired images were uploaded onto an MBF Workstation (MBF Biosciences), and the number of activated microglia was quantified by counting ED-1⁺-positive cell bodies (black on nuclear fast red counterstained background) using the Optical Fractionator probe and systemic random sampling according to unbiased stereological principles. All analyses were conducted blind from coded slides (9–12 brain sections per animal, $n = 3$ animals per group). Sampling parameters (grid and counting frame size) were empirically determined to achieve low coefficients of error (Gundersen’s CE, $\leq 0.06 \pm 0.01$, $n = 4$) for each region of interest.